

Gas phase potassium release from a single particle of biomass during high temperature combustion

Patrick E. Mason, Jenny M. Jones*, Leilani I. Darvell, Alan Williams

School of Chemical and Process Engineering (SCAPE), University of Leeds, Leeds LS2 9JT, UK

Received 2 December 2015; accepted 4 June 2016

Available online 21 June 2016

Abstract

A notable characteristic of solid biomass fuels as compared to coal is their significantly higher potassium content. Potassium influences ash deposition and corrosion mechanisms in furnaces and boilers, the effects of which may differ depending on phase transformations of potassium species in the gas phase and condensed phase. An understanding of how potassium is released from biomass fuels during the combustion process is therefore useful for plant designers and operators assessing means of avoiding or mitigating these potential problems. An experimental method is used to measure release patterns from single particles of biomass fuels using flame emission spectroscopy and a single-particle combustion rig. The experimental arrangement also allowed simultaneous thermal imaging of the combusting particle in order to determine the surface temperature. A model of the single particle combustion is presented. Using experimental data on devolatilisation and burnout times for different sized particles and the measured surface temperature profiles, the thermal and kinetic sub-models are verified. A model for potassium release is described and this is integrated to the single particle combustion model to allow prediction of the temporal patterns of release of gas-phase potassium. The modelled release patterns were compared with those observed. Good agreement between modelled and measured potassium release patterns was attained confirming that the proposed mechanisms affecting potassium release are valid.

© 2016 by The Combustion Institute. Published by Elsevier Inc.

Keywords: Biomass; Combustion; Single-particle; Modelling; Potassium

1. Introduction

Combustion of solid biomass fuels, as an alternative to coal in large-scale combustion plant, or in dedicated boilers, introduces various challenges to operators. In particular, certain biomass materials have ash compositions which introduce

problems of fouling, slagging and corrosion issues. Biomass fuels contain variable proportions of potassium, a key plant nutrient, and this is one of the more significant components affecting ash behaviour. Potassium is associated with both the organic and inorganic fractions in the biomass [1]. Because of the importance of K-partitioning in combustion systems, various research teams have sought to measure and model its behavior [1–5]. Some is released during pyrolysis, possibly

* Corresponding author.

E-mail address: j.m.jones@leeds.ac.uk (J.M. Jones).

entrained in the volatiles, and some of the inorganic potassium evolves as KOH or KCl to the gas phase during combustion temperatures. This partitioning is followed by gas phase reactions and deposition of potassium aerosols in convective sections of the boiler, where corrosive deposits are formed. The potassium that remains in the solid phase impacts on ash behavior and influences both fouling and slagging in the furnace.

Modelling of combustion and predicting ash behavior is essential in boiler design and requires effective sub-models [6] specific to biomass. Woody and herbaceous biomass materials are anisotropic, non-homogeneous and there is a natural variation in physical and chemical characteristics even within samples from the same source. It is therefore important to recognise that any model must be of an idealised version of the actual material. In the case of modelling heat transfer, the particle shape is often idealised to quasi-spherical, even though in most cases biomass particles tend to be more quasi-cylindrical. This allows mathematical models to be simplified to one-dimensional systems such as described by Porteiro et al. [7] and Haseli et al. [8]. Others have adopted two-dimensional models to account for the effects of shape such as that described by Yang et al. [9].

Since the thermal conductivity of biomass is low in relation to particle sizes and heating rates in the relevant applications, accounting for internal heat transfer is an important consideration [10]. The effects of particle size and shape and the associated internal temperature gradients on thermal conversion have been investigated by Lu et al. [11] and illustrated with experimental data on relatively large particles (~11 mm diameter). Internal thermal gradients may be approximated using idealised analytical equations. However, to practically account for the intrinsic thermal effects of combustion reactions, numerical methods are necessary. One approach is to consider the particle as comprising of a series of concentric, discrete layers such that heat flow and mass transfer from the surface to the center and vice-versa can be accounted for. Such an approach has been adopted by Thunman et al. [12] and Porteiro et al. [7]. The approach to single particle combustion modelling described is also applicable to modelling the evolution of inorganic species during the combustion process.

Experimental studies on potassium release from biomass combustion have shown that evolution of potassium to the gas-phase is highly dependent on the particle temperature and higher proportions of potassium are released in the latter stages of the char combustion [2,13–15]. Previous modelling of potassium release during single particle combustion assumed a small fraction of the potassium (<15%) is released at the same rate as pyrolysis, and the volatile inorganic potassium was described by an evaporation model [2]. This paper extends

Table 1
Composition of selected biomass fuels.

Content	Basis	Units	Pine	Willow
Moisture	a.r.	%wt	8.3	6.0
Ash	dry	%wt	2.0	2.0
Volatile	daf	%wt	82.5	83.6
Char	daf	%wt	17.5	16.4
GCV	dry	MJ kg ⁻¹	18.6	19.8
Elemental				
C	daf	%wt	47.4	50.8
H	daf	%wt	5.3	6.0
O	daf	%wt	45.9	42.7
N	daf	%wt	1.3	0.4
K	dry	%wt	0.12	0.21

our previous work in modelling the phase transformation of potassium species to the gas phase. The model is derived from, and validated by single particle combustion measurements [16,17]. In this extended model, the prediction of potassium release is closely linked to the prediction of temperature of the combusting particle and the concentration of potassium during the progressing stages of combustion. The model accounts for internal thermal effects and is used as a basis to predict gas-phase potassium release. The results of the model are compared to experimental data including the measured particle surface temperature and the observed potassium release.

2. Experimental method

2.1. Biomass fuel samples, characterisation and preparation

Two woody biomass materials are investigated: pine and willow. The pine is representative of the typical “white wood” commonly used in many biomass furnaces. The willow is a UK short rotation coppice energy crop. The fuels were characterised using CEN standard procedures for determining composition as summarised in Table 1. While the speciation of potassium in the solid phase is uncertain, at the temperature of the flame (1800 K) the stable gas-phase species are KCl and KOH [18]. For both samples, chlorine measurements were at the limit of measurement errors (<0.05 %wt). For the purposes of modelling, it was estimated that potassium volatilised predominantly in the form of KOH with around 25% KCl. Individual samples of biomass (~0.5–4 mm in length) were prepared as regular cuboid-shaped particles and the volume, mass and density of each particle were recorded. A separate set of willow particles were prepared with known quantities of potassium by means of doping with a solution of potassium acetate to give potassium content (by mass)

of 0.1%, 0.25%, 0.5% and 0.75%. These were used as reference samples for model validation.

2.2. Single particle combustion apparatus

The experimental apparatus consists of a means of suspending a single particle in a methane flame using a technique used in previous studies [2,17]. This is achieved by impaling the particle on a fine needle supported over a Méker gas-burner. The sample is shrouded in a water-cooled sleeve which shields the particle from the gas flame until the instant of withdrawal and the start of the combustion process is initiated. The measured gas flame temperature was 1800 K and the oxygen concentration was 10.7%

2.3. Thermal imaging

A FLIR SC640 thermal imaging camera with a 373–2273 K measurement range was used to record the surface temperature of the particle. The surface temperature profile of each particle was extracted from a recorded image in post-experiment analysis. The emissivity for temperature measurement and modelling is estimated at 0.85. This value is based on reported experimental values for both wood and char [19].

2.4. Gas-phase potassium detection

At gas temperatures of 1700 K to 1800 K, potassium in species released to the gas phase are thermally excited such that the intensity of spectral emission is taken to be proportional to the concentration of volatilised potassium in the flame. Using an optical band-pass filter to select the 766 nm spectral emission of potassium with a linear-response photo-diode detector, the relative concentration in the hot gas flow above the combusting particle could be recorded. The detector was mounted at fixed position for imaging part of the flame directly above the particle. This measurement technique provided time-history profiles of the relative rate of potassium release for the entire duration of the single particle combustion. Further details of the experimental method are presented in previous studies [16].

3. Modelling method

A model of the single particle combustion has been developed using established heat transfer models and mass loss models based on single-step combustion kinetics. The principal equations used for the various aspects of the model are summarised in Table 2.

In order to adequately represent the internal heat transfer and mass loss in the particle interior,

the particle is modelled as a series of discrete concentric layers of 100 μm . The heat and mass calculations for each layer are performed at discrete time steps of 1 μs . The model was realised in a FORTRAN code.

3.1. Heat transfer

The convective surface heat transfer is calculated using fluid dynamic models relating the gas to a spherical particle (Eqs. 1–4). The radiative heat loss (Eq. 5) is calculated with an emissivity of 0.85 and ambient temperature of 300 K as in the experimental conditions. Internal heat transfer is calculated as thermal conduction between concentric layers of the modelled particle (Eq. 6).

3.2. Mass loss

As the particle heats up, each layer undergoes a process of drying, devolatilisation and finally, char combustion. Each of these processes is modelled with respect to the calculated temperature of the respective layer. Moisture mass loss is calculated with a water evaporation model (Eq. 7). Devolatilisation and char combustion are calculated with single step first order Arrhenius kinetic reaction models (Eqs. 9 and 11). The parameters for these models (frequency factor and activation energy) were selected in the first instance from thermogravimetric measurements on finely milled (<90 μm particle size) samples of each material at low heating rates (10 K/s). The observed devolatilisation and burn-out times in the experiment were used to determine the apparent frequency factors (A_{vol} and A_{chr}) assuming apparent first order reactions in each case. The resulting values as used in the model are presented in Table 3. These values compare agreeably with other published kinetic parameters for biomass [20,21].

The calculated mass loss for each layer of the model is used to derive the changing nature of the particle as it undergoes combustion. The volume of each layer is recalculated at each step based on the density of the char particle only such that no change in volume results from loss of volatile matter but shrinkage of the particle occurs as the char mass is consumed. The changes in particle volume and density are approximations based on experimental observations of combusting single particles [17].

3.3. Internal energy balances

The mass losses from each of the modelled processes described above have associated thermal effects. The effect of moisture evaporation is modelled as a heat loss at the surface of the particle based simply on the enthalpy of vapourisation of the respective mass of water (Eq. 8). Similarly, the effect of volatile vapour emission is modelled as

Table 2
Principal mathematical models.

Quantity	Model	Eqn	Model variables and constants	
Reynolds number	$Re = D \cdot \frac{U_{gas}}{v_{gas}}$	(1)	D	particle diameter
Nusselt number	$Nu = 2 + (0.6 \sqrt{Re} \sqrt[3]{Pr})$	(2)	$U_{gas} = 2.5 \text{ m s}^{-1}$	gas velocity
convective heat transfer coefficient	$H_{conv} = \frac{Nu \cdot \lambda_{gas}}{D}$	(3)	$v_{gas} = 3.0 \times 10^{-4} \text{ m}^2 \text{ s}^{-1}$	gas kinematic viscosity
convective heat transfer to surface layer	$dQ_{conv} = S_L H_{conv} (T_{gas} - T_s) \cdot dt$	(4)	$Pr = 0.71$	Prandtl number for gas
Radiative heat transfer to surface layer	$dQ_{rad} = S_L \varepsilon \sigma (T_R^4 - T_s^4) \cdot dt$	(5)	$\lambda_{gas} = 0.122 \text{ Wm}^{-1}\text{K}^{-1}$	gas thermal conductivity
Internal conductive heat transfer	$dQ_{cond} = S_L \lambda_L \frac{\Delta T_L}{\Delta r_L} \cdot dt$	(6)	S_L	outer surface area of layer
Moisture evaporation - mass loss	$\frac{dm_w}{dt} = \chi (T_L - T_{eq}) m_w$	(7)	$T_{gas} = 1800 \text{ K}$	gas flame temperature
Moisture evaporation - heat loss	$dQ_{evap} = dm_w H_{evap}$	(8)	T_s	particle surface temperature
Devolatilisation - mass loss	$\frac{dm_{vol}}{dt} = -m_{vol} A_{vol} e^{\left(\frac{-E_{vol}}{RT_L}\right)}$	(9)	$\varepsilon = 0.85$	particle surface emissivity
Devolatilisation - heat loss	$dQ_{vol} = dm_{vol} H_{vol}$	(10)	$\sigma = 5.67 \times 10^{-8} \text{ Wm}^{-2}\text{K}^{-4}$	Stefan-Boltzmann constant
Char oxidation - mass loss	$\frac{dm_{chr}}{dt} = -m_{chr} \Phi_{O_2}^n A_{chr} e^{\left(\frac{-E_{chr}}{RT_L}\right)}$	(11)	T_R	ambient surface temperature
Oxygen diffusion	$dm_{O_2(D)} = -\Gamma_{O_2} S_L \frac{\Delta \Phi_{O_2}}{\Delta r_L} \cdot dt$	(12)	$\lambda_L = 0.14 \text{ Wm}^{-1}\text{K}^{-1}$	thermal conductivity of layer
Char oxidation - heat gain	$dQ_{chr} = dm_{chr} H_{chr}$	(13)	T_L	particle layer temperature
Temperature change in layer	$dT_L = \frac{Q_{net,L}}{m_L C_P}$	(14)	Δr_L	radial thickness of layer
Concentration of gas phase potassium in layer	$\Phi_{K(g)} = \frac{\alpha_K m_K}{V_L} \cdot e^{\left(\frac{-H_K}{RT_L}\right)}$	(15)	m_w	mass of moisture in the layer
Potassium release by entrainment	$dm_{K(E)} = -\beta \cdot \Phi_{K(g)} \cdot dm_{vol}$	(16)	$\chi = 0.0925$	evaporation rate coefficient
Potassium diffusion coefficient	$\Gamma_K = 4.3 \times 10^{-11} T_L^{1.76}$	(17)	$T_{eq} = 310 \text{ K}$	evaporation threshold temperature
Potassium diffusion	$dm_{K(D)} = -\Gamma_K S_L \frac{\Delta \Phi_{K(g)}}{\Delta r_L} \cdot dt$	(18)	$H_{evap} = 2.26 \times 10^6 \text{ J kg}^{-1}$	enthalpy of water evaporation
			m_{vol}	mass of volatile matter
			A_{vol}	devolatilisation reaction freq. factor
			E_{vol}	devolatilisation activation energy
			$R = 8.31 \text{ J mol}^{-1}\text{K}^{-1}$	gas constant
			$H_{vol} = -0.2 \times 10^6 \text{ J kg}^{-1}$	enthalpy of vaporization of volatiles
			m_{chr}	mass of char
			A_{chr}	char reaction frequency factor
			E_{chr}	char reaction activation energy
			Φ_{O_2}	relative concentration of O_2 in layer
			$n = 0.75$	reaction order with respect to O_2
			$\Gamma_{O_2} = 2.5 \times 10^{-5} \text{ m}^2 \text{ s}^{-1}$	diffusivity of oxygen in char
			$H_{chr} = 12.7 \times 10^6 \text{ J kg}^{-1}$	enthalpy of char oxidation reaction
			$Q_{net,L}$	net heat flux into layer
			m_L	mass of particle layer
			C_P	specific heat capacity of layer
			m_K	mass of potassium in layer
			$\alpha_K = 0.065$	gas-phase potassium coefficient
			V_L	volume of layer
			H_K	K-species vaporisation enthalpy
			$\beta = 1.0 \times 10^{-3} \text{ m}^3 \text{ kg}^{-1}$	entrainment coefficient
			d	differential operator (for time steps)
			Δ	differential operator (across layers)

Table 3
Parameters of kinetic models used for devolatilisation and char combustion.

	Reaction kinetic coefficients			
	$A_{\text{vol}} \text{ (s}^{-1}\text{)}$	$E_{\text{vol}} \text{ (kJ.mol}^{-1}\text{)}$	$A_{\text{chr}} \text{ (s}^{-1}\text{)}$	$E_{\text{chr}} \text{ (kJ.mol}^{-1}\text{)}$
<i>Pine</i>				
TGA derived	1.1×10^3	61	1.1×10^5	92
Modelled	8.0×10^3	61	4.0×10^4	92
<i>Willow</i>				
TGA derived	6.0×10^2	58	6.0×10^4	92
Modelled	4.0×10^3	58	1.8×10^5	92

a heat loss at the surface (Eq. 10). The exothermic char combustion is modelled as a heat gain internally for each layer (Eq. 12). The temperature change at each time step is then calculated from the net heat flux in each layer and its respective heat capacity.

3.4. Potassium release

Three stages of potassium release during biomass combustion were identified by Jones et al. [2] which coincide with the different stages of thermal decomposition and combustion of the particle, namely: devolatilisation, char combustion and ash decomposition. The direct vapourisation of K-species from the biomass particle is governed by the respective vapour pressures of KCl and KOH. These can be modelled [18] as functions of temperature and vapourisation enthalpy: 164 kJ/mol and 147 kJ/mol respectively [22,23]. The concentration of gas-phase KOH and KCl is then derived using Eq. (15) from the respective solid-phase mass, temperature and volume in each layer of the model. Fatehi et al. [13] have shown that overall potassium release rate observed in similar experiments can be modelled as a first order Arrhenius expression: essentially a temperature-dependent relationship of the same form as presented in this study.

3.4.1. Devolatilisation stage

The mechanisms for the release of potassium in to the gas phase during the initial devolatilisation stage of combustion are: (i) direct vapourisation of inorganic potassium (KCl and KOH); (ii) dissociation of potassium from the combustion of organic volatiles released by pyrolysis. The latter of these is more significant in lower temperature pyrolysis processes as described by Yu and Zhang [1] while, at higher temperatures there is higher vapourisation of the inorganic species and the former dominates. The evaporation rate is a function of the concentration of gas-phase potassium and the rate at which the vapour is removed by either diffusion or convective mass transfer. In the devolatilisation stage, a strong convective mass transfer mechanism is provided by the Stefan flux resulting from

the generation of gas-phase organic volatiles inside and at the surface of the particle. This flux will entrain the evaporated potassium species as well as any potassium bound to the organic species themselves. The release of potassium in the devolatilisation stage will then be related to both the rate of devolatilisation and the gas-phase potassium concentration both of which are functions of temperature.

3.4.2. Char combustion stage

In the char combustion stage, the mass transfer mechanism for the release of potassium is governed by diffusion in the gas phase. The rate of release by diffusion can be modelled with Fick's law for a spherical system, where the flux through the surface of the particle is proportional to the radial concentration gradient at the surface, the diffusivity coefficient Γ and the surface area.

The concentration gradient at the surface of each layer is modelled as simply the difference between the calculated gas-phase concentration of KOH and KCl and radial distance between successive layers. The external concentration outside the particle is taken to be zero so the release rate from the particle surface is then directly proportional to the concentration in the outer layer.

3.4.3. Ash decomposition stage

Depending on other inorganics in the ash (e.g. silica), high temperature combustion may release virtually all the potassium to the gas phase by the end of the char combustion stage. There is a general finding that this is true for materials with relatively low potassium content, while, for materials with higher potassium content, a significant amount of potassium is retained in the ash particle [16]. If the ash particle continues to be exposed to the high temperature flame, potassium continues to be released to the gas phase. In the case of this experiment, there is an abrupt transition at the point of char burnout where the increase in particle temperature resulting from the char oxidation ceases. Thereafter, the particle temperature is constant and the potassium release rate declines as the remaining content is diminished.

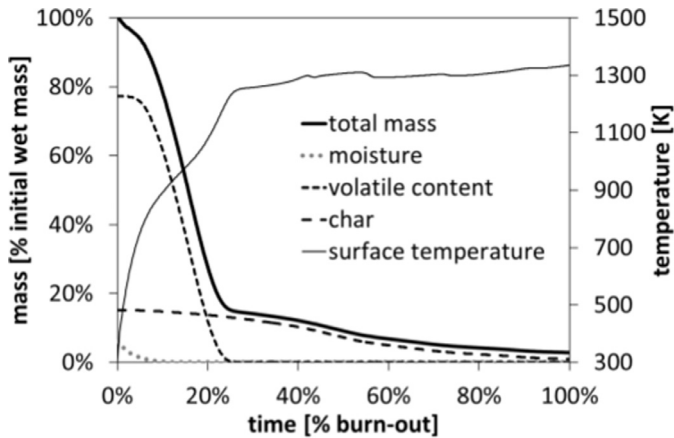


Fig. 1. Example modelled combustion mass-loss time-history (for 4.9 mg willow particle).

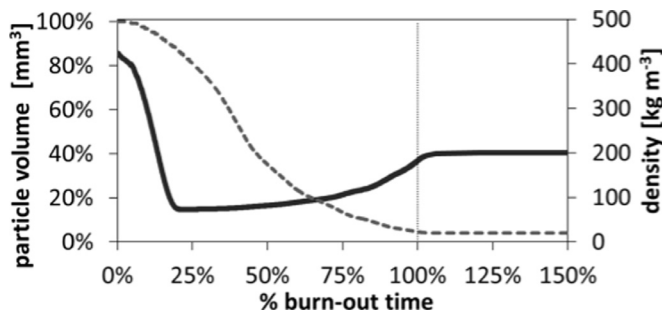


Fig. 2. Example modelled volume (dashed line) and density (solid line) time-history (4.9 mg willow particle).

4. Results

An example of the modelled particle mass-loss history is presented in Fig. 1. The form of these is similar for both materials and compares well with mass-loss curves for wood particles combustion in high temperature furnaces as produced by Li et al. [24] using a CFD combustion model. From these profiles, the predicted durations of the devolatilisation and full burnout can be derived.

The changes in volume and density of the particle during each stage of combustion are illustrated by Fig. 2. The changes correspond to the transitions between the stages of combustion: a steady decrease in density during devolatilisation; a shrinking volume during char combustion; an increase in density as the char/ash coalesces and constant volume and density of ash particle thereafter.

In previous experimental studies [17] on single particle combustion, devolatilisation and char burnout durations were measured for many particles of solid biomass with dry mass in the range of 1–20 mg. Analysis of the data showed a power-function relationship between the duration (t) of

various stages of combustion and particle mass (m) of the form: $t = am^b$. This is illustrated in Fig. 3, which shows experimental data for the willow compared with the modelled combustion times. The model output conforms to the power-function form of the relationship between particle mass and combustion time. This measured data was used to determine the effective kinetic parameters (see Table 3) in the model.

The change in surface temperature of the modelled particle is affected by different parameters. The external heat transfer is sensitive to the assumed emissivity and the fluid dynamical modelling of the hot gas flame. Internal heat transfer is affected by the thermal conductivity and heat capacity in each model layer. There is also a strong influence on the particle surface temperature from heat of vapourisation whereby the rate of devolatilisation determines a surface cooling effect.

Modelled surface temperature time-histories are presented in Fig. 4 together with the respective surface temperatures measured using a thermal imaging camera. There is a satisfactory agreement between the model and the measured data. The

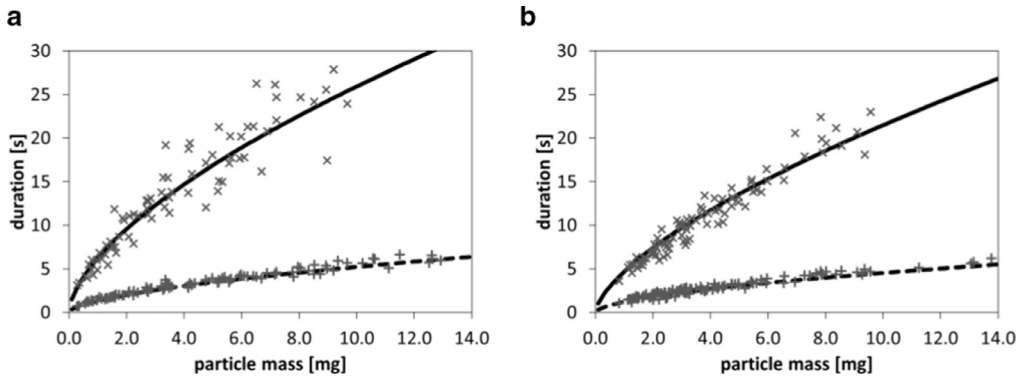


Fig. 3. Comparison of modelled devolatilisation (dashed line) and burn-out times (solid line) compared with experimental data (symbols + and x respectively) for: (a) pine; (b) willow.

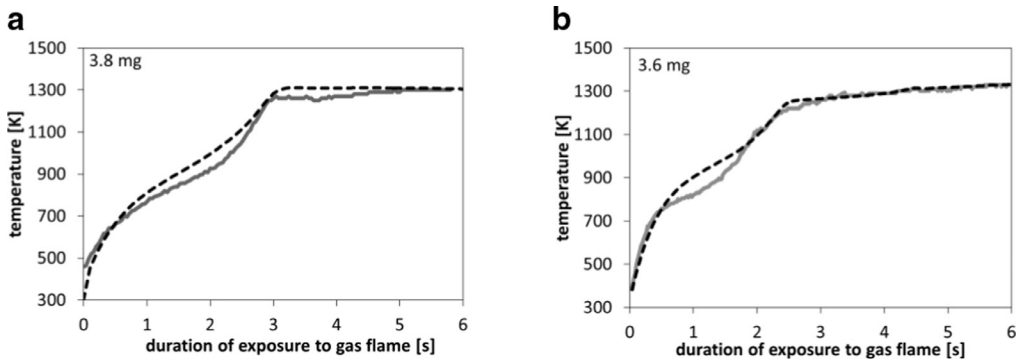


Fig. 4. Modelled particle surface temperature (dashed line) compared to measured surface temperature (solid line) for: (a) pine; (b) willow.

effects of the devolatilisation stage on retarding the rise in surface temperature is observed in the measured profile and this is replicated in the model. Following devolatilisation, the surface temperature reaches around 1300 K and increases more slowly as the char combustion proceeds.

The modelling of the chemical kinetics, thermodynamics and the changes in particle volume and density described thus far all have effects on the release rate of the gas-phase potassium in the particle. By integrating the potassium release model into the combustion model all these effects are accounted for.

A means of validating certain aspects of the model is to simulate the potassium release for the test samples of willow doped with known quantities of potassium. The model was run with the same parameters for the willow model and with potassium concentrations (by mass) of 0.1%, 0.25%, 0.5% and 0.75% respectively – corresponding to the concentrations in the doped willow particles used as reference samples. Averaged release profiles from at least 3 particles for each doped sample were recorded. These are shown in Fig. 5 together with

the modelled release profiles. The comparison with the reference samples confirms key features of the release patterns: (i) the total potassium release (area under the line) is proportional to the total potassium content; (ii) the peak release rate is approximately proportional to the potassium content; (iii) qualitatively, the general shape of the release profiles are similar.

Figure 6 shows the recorded potassium release profiles for particles of the willow and pine samples together with the modelled profiles for comparison. The general features of the modelled potassium release pattern correspond to those as observed. In the devolatilisation stage, there is relatively little release but nevertheless, a minor peak in the release rate is seen from potassium entrained in the released volatiles. The char combustion stage is characterised by a steady increase in the release rate to a distinct peak. The release mechanism in this stage is modelled entirely as diffusion of the volatilised KOH and KCl. The shape of the peak implies an accelerated release of potassium near to the end of char burnout. In the model, this is replicated and is a consequence of increased particle temperature

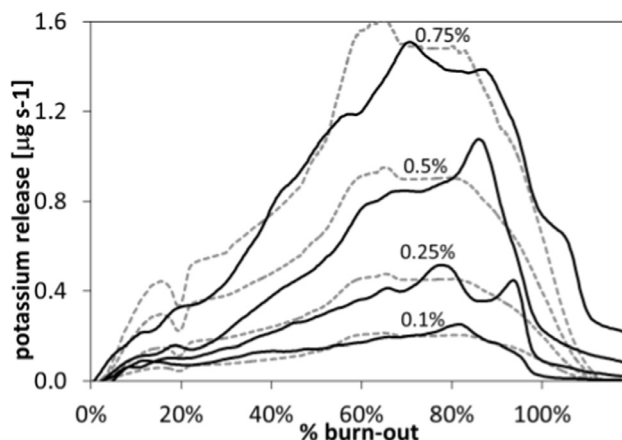


Fig. 5. Averaged potassium release profiles for doped willow particles: measured (solid lines) compared to modelled release profiles (dashed lines).

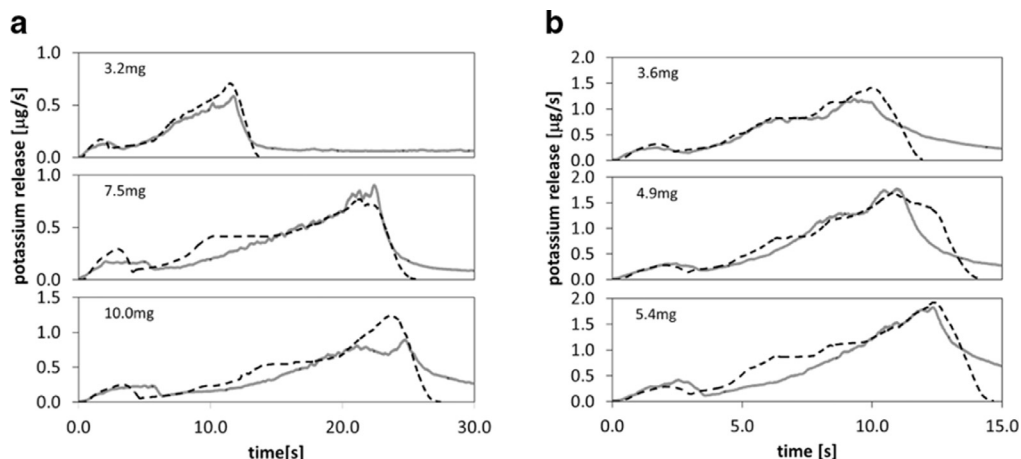


Fig. 6. Modelled (dashed lines) and measured (solid lines) potassium release profiles for particles of: (a) pine; (b) willow.

and the transition to a smaller, denser particle at the end of char combustion, increasing the gas-phase KOH+KCl concentration in the particle.

The peak is followed by a rapid decay. The model shows a complete decay to zero in a short period whereas the measured pattern shows an ongoing low level of release for an extended period. It is inferred from this that there is a different mechanism of release from the ash particle.

The model shows the peak release close to that of the observed release pattern. The willow and pine have different potassium content (0.21 and 0.12 %wt respectively), and this is reflected in the respective peak release rate indicating that release rate is a direct function of the concentration of potassium in the particle. The variation of the average potassium volumetric concentration in the combusting particle is illustrated in Fig. 7.

5. Conclusions

The capability of predicting the release of potassium to the gas phase during the combustion of biomass in large scale furnaces is useful for understanding the ash fouling and corrosion potential of various fuels. Since the thermal, kinetic and physical changes that occur during combustion all influence the rate of potassium release, it is important that modelling accounts for as many of these aspects as practical. It has been shown that single-step kinetic models for devolatilisation and char oxidation together are effective in modelling the mass loss as a function of particle temperature. Heat and mass transfer internal to the particle are effectively modelled using a spherical approximation with discrete concentric layers. Using data from laboratory-scale experiments, the modelling of devolatilisation

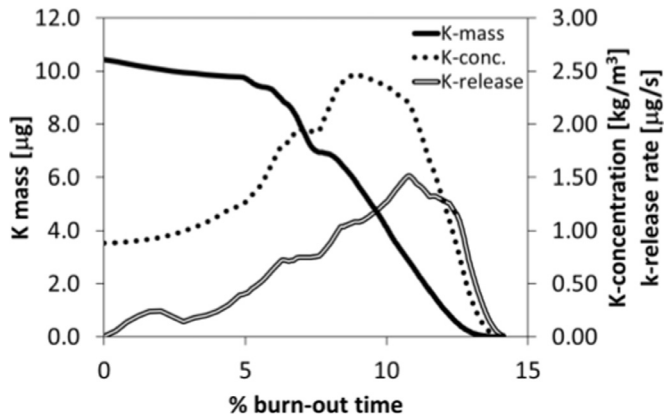


Fig. 7. Modelled variation in average volumetric concentration, mass and release rate of potassium from a combusting particle of willow (4.9 mg).

and burnout have been validated. The predicted surface temperature time-profile has also been validated using measurements derived from thermal imaging. In addition, contemporaneous measurements of the potassium release rate taken using a flame spectroscopy technique have shown temporal release patterns which display a generic form close to that of the model. Three stages of potassium release coincident with the stages of combustion (devolatilisation, char oxidation and ash decomposition) are demarcated by changes in particle density. The model confirms the effects that potassium concentration, temperature and density all have on the observed patterns of potassium release. The potassium release sub-model described may be applied to other biomass where the potassium content and the combustion kinetics are known. Further development of the model is possible for replicating the release/retention of gas-phase potassium from the ash particle.

Acknowledgements

The authors are grateful for financial support from Research Councils UK (Grant EP/K02115X/1). P.E. Mason thanks The University of Leeds for the award of a postgraduate scholarship.

References

- [1] C. Yu, W. Zhang, in: A.V. Bridgewater (Ed.), *Progress in Thermochemical Biomass Conversion*, Vol. 2, Blackwell Science, Oxford, 2001, pp. 1107–1115.
- [2] J.M. Jones, L.I. Darvell, T.G. Bridgeman, M. Pourkashanian, A. Williams, *Proc. Combust. Inst.* 31 (2007) 1955–1963.
- [3] P.A. Jensen, F.J. Frandsen, K. Dam-Johansen, B. Sander, *Energy Fuels* 14 (2000) 1280–1285.
- [4] J.G. Olsson, U. Jaglid, J. Pettersson, P. Hald, *Energy Fuels* 11 (1997) 779–784.
- [5] J.G. Olsson, J. Pettersson, N. Padban, I. Bjerle, *Energy Fuels* 12 (1998) 626–630.
- [6] L. Ma, J.M. Jones, M. Pourkashanian, A. Williams, *Fuel* 86 (12–13) (2007) 1959–1965.
- [7] J. Porteiro, J.L. Míguez, E. Granada, J.C. Moran, *Fuel Process. Technol.* 87 (2) (2006) 169–175.
- [8] Y. Haseli, J.A. van Oijen, L.P.H. de Goeij, *Bioresour. Technol.* 102 (20) (2011) 9772–9782.
- [9] Y.B. Yang, V.N. Sharifi, J. Swithenbank, et al., *Energy Fuels* 22 (1) (2008) 306–316.
- [10] A.N. Hayhurst, *Combust. Flame* 160 (1) (2013) 138–144.
- [11] H. Lu, E. Ip, J. Scott, P. Foster, M. Vickers, L.L. Baxter, *Fuel* 89 (5) (2010) 1156–1168.
- [12] H. Thunman, B. Leckner, F. Niklasson, F. Johnsson, *Combust. Flame* 129 (1–2) (2002) 30–46.
- [13] H. Fatehi, Y. He, Z. Wang, et al., *Proc. Combust. Inst.* 35 (2) (2015) 2389–2396.
- [14] Z.-H. Zhang, Q. Song, Z.T. Alwahabi, Q. Yao, G.T. Nathan, *Combust. Flame* 162 (2) (2015) 496–505.
- [15] T. Sorvajärvi, N. DeMartini, J. Rossi, J. Toivonen, *Appl. Spectrosc.* 68 (2) (2014) 179–184.
- [16] P.E. Mason, L.I. Darvell, J.M. Jones, A. Williams, *Fuel* 182 (2016) 110–117.
- [17] P.E. Mason, L.I. Darvell, J.M. Jones, M. Pourkashanian, A. Williams, *Fuel* 151 (2015) 21–30.
- [18] H.M. Westberg, M. Byström, B. Leckner, *Energy Fuels* 17 (2003) 18–28.
- [19] J. Salinero, A. Gómez-Barea, M. Tripijana, B. Leckner, *Chem. Eng. J.* 288 (2016) 441–450.
- [20] A. Saddawi, J.M. Jones, A. Williams, M.A. Wójtowicz, *Energy Fuels* 24 (2010) 1274–1282.
- [21] P. McNamee, L.I. Darvell, J.M. Jones, A. Williams, *Biomass Bioenergy* 82 (2015) 63–72.
- [22] P.C.R. Rodrigues, F.M.S. Silva Fernandes, *J. Chem. Phys.* 126 (2) (2007) 024503.
- [23] L.V. Gurvich, G.A. Bergman, L.N. Gorokhov, V.S. Iorish, V.Y. Leonidov, V.S. Yungman, *J. Phys. Chem. Ref. Data* 25 (4) (1996) 1211–1276.
- [24] J. Li, M.C. Paul, P.L. Younger, I. Watson, M. Hossein, S. Welch, *Energy Procedia* 66 (2015) 273–276.